https://doi.org/10.5194/wes-2026-20
Preprint. Discussion started: 16 February 2026

eawe european academy of wind energy
Open Access WIND ENERGY SCIENCE DISCUSSIONS

Offshore wind profile characteristics and their impact on floating wind turbine power production

Nikolas Angelou[1] and Camille Dubreuil-Boisclair[2]

[1]Technical University of Denmark (DTU), Frederiksborgvej 399, Roskilde, 4000, Denmark
[2]Equinor ASA, Sandslivegen 90, Sandsli, 5254, Norway

Correspondence: Nikolas Angelou (nang@dtu.dk)

Abstract. In this study, we investigate the impact of vertical wind shear and wind speed inversions on the power production of a floating offshore wind turbine. Using nacelle-mounted wind lidar data from a 6 MW turbine at the Hywind Scotland wind farm, we analyse inflow conditions and turbine performance during summer and autumn. The wind climatology shows that 33% of examined cases exhibit non-standard wind profiles within the rotor-swept area, including negative shear and wind speed inversions. These conditions significantly affect power production, particularly below rated wind speeds, with negative shear profiles causing reductions of up to 20% compared to the reference power curve. Our findings demonstrate that deviations from the logarithmic wind profile at the operating height range of modern wind turbines, are frequent in deep-water offshore environments and can introduce substantial bias in power curve verification. Nacelle-mounted wind lidars provide critical insight into these inflow characteristics, enabling improved performance assessment of floating offshore wind turbines. The results highlight the need for measurement strategies that capture wind conditions across the full rotor-swept area, which can be achieved through nacelle-mounted wind lidar instruments.

1 Introduction

Offshore wind conditions offer significant potential for renewable energy production. Sea surface characteristics, such as low friction and high spatial homogeneity, result in wind conditions typically characterised by low atmospheric turbulence levels and high spatial isotropy. These conditions favour the development of large wind turbines with high power production capacity. However, as the operating height of wind turbines increases, the wind field they interact with may exhibit a vertical profile with negative shear or wind speed inversion. These features can occur, for example, in a shallow atmospheric boundary layer or in the presence of a low-level jet (LLJ) Peña et al. (2008); Hallgren et al. (2023). Such wind conditions are relevant for the operation of offshore wind farms, as they can affect wind turbines both in terms of power production and aerodynamic loads Gutierrez et al. (2017); Doosttalab et al. (2020); Gadde and Stevens (2021). Until today it is still challenging to predict the

https://doi.org/10.5194/wes-2026-20
Preprint. Discussion started: 16 February 2026

eawe european academy of wind energy
Open Access WIND ENERGY SCIENCE DISCUSSIONS

characteristics of these wind profile events using mesoscale and reanalysis (e.g. Nunalee and Basu, 2014; Olsen et al., 2024; Bui et al., 2025), which highlight th need for more observational studies of offshore wind profiles Shaw et al. (2022).

Measuring offshore wind conditions is a challenging task. The depth of the ocean floor makes the installation of meteorological masts technically demanding and costly. For this reason, tall ($\geq$ 100 m) offshore masts equipped with in-situ wind sensors are currently installed only at two locations in the North Sea and one in the Baltic Sea (i.e. FINO – Research platforms in the North Sea and Baltic Sea FINO (2025)). The height range of meteorological masts can be extended through the use of remote-sensing ground-based wind profilers, which can be installed on fixed (e.g. Peña et al., 2008; Kim et al., 2019; Bui et al., 2025) and floating (e.g. Foussekis and Mouzakis, 2021) platforms that support masts. A paradigm shift in measuring offshore wind profiles was introduced with the development of floating wind lidar profilers, i.e. Doppler lidars installed on buoys Gottschall et al. (2017). Floating wind lidars have been shown to measure mean wind speed at different heights accurately (e.g. Peña et al., 2022) and thus used to study offshore wind profiles (e.g. Debnath et al., 2021).

A promising option for expanding the wind energy sector, despite the need for further technological developments Robertson et al. (2025), is floating offshore wind turbines (FOWTs). However, assessing the operation of this concept is challenging, as it relies on the interaction between ambient wind conditions, sea state, and the corresponding motion induced in a FOWT during operation. FOWTs experience motion in six degrees of freedom while operating: three rotational (roll, pitch, and yaw) and three translational movements (surge, sway, and heave). Currently, there is increasing interest within the wind energy research community in assessing the impact of the motions induced on a FOWT during operation on power production (e.g. Couto et al., 2022; Fontanella et al., 2024). This topic has been primarily investigated through wind tunnel experiments and computational fluid dynamics simulations. Due to the complexity of this problem, researchers usually decouple the FOWT motions and investigate their impact separately Sant et al. (2015); Wen et al. (2017); Li et al. (2018); Wen et al. (2018a, b); Fu et al. (2019). However, to date, only a few studies have examined the power production of utility-scale FOWTs operating in natural atmospheric and sea-state conditions (e.g. Özinan et al., 2022). Thus, it is still unclear the aggregated effect that the motions over six degrees of freedom have on the power production of a FOWT.

The study of a utility-scale wind turbine's power production is based on the Power Curve Verification (PCV) procedure described by the International Electrotechnical Committee IEC 61400-12-1 (2022). Offshore wind conditions tend to reduce complications in performing PCV compared to onshore, as the sea state is spatially homogeneous. However, as discussed previously, variations in the vertical wind speed gradient at the top of the rotor create a need to observe the wind profile not only at hub height but across a wide range of altitudes spanning the rotor plane. In general, the impact of shear on power production has been identified in onshore fixed-bottom wind turbines, for the case of vertical wind speed variations close to the ground (Wagner et al., 2009). For this reason, especially in those cases where the vertical variations of wind speed deviates from a height-dependent logarithmic profile, it is recommended to use a Rotor Equivalent Wind Speed (REWS) (Wagner et al., 2011). The use of nacelle-mounted wind lidars,which operates while mounted on a wind turbine's nacelle, offers great potential for performing PCV for mainly two reasons. First, the optical axis[1] of nacelle-mounted wind lidars follows the yaw direction of the nacelle, thus maximising data availability (Wagner et al., 2014b), and second since they provide measurements at different

[1]The term optical axis is used here to denote the axis relative to which the geometry of the line-of-sight measurements is defined.

https://doi.org/10.5194/wes-2026-20
Preprint. Discussion started: 16 February 2026

heights, necessary for the estimation of a REWS. This makes nacelle-mounted wind lidars an alternative option to floating wind lidars for offshore measurements, in the context of a PCV. A complication in applying PCV using a nacelle-mounted wind lidar to a FOWT is that the optical axis of the wind lidar is subject to floater dynamics, requiring a motion-correction procedure Gräfe et al. (2023).

This study presents a spatio-temporal characterisation of offshore wind profiles that exhibit a wide range of wind shear values, including wind speed inversions along the rotor. For this purpose, we use data covering the summer and autumn periods, acquired by a nacelle-mounted wind lidar installed on a FOWT at Hywind Scotland—the first commercial floating offshore wind farm (Jacobsen and Godvik, 2021), located on the eastern coast of Scotland in the North Sea, an area with high wind energy potential (Hahmann et al., 2023). As already discussed, nacelle-mounted wind lidars offer an attractive method for studying offshore wind conditions, as they can provide estimates of various parameters describing the wind field interacting with large wind turbines (e.g. Angelou et al., 2023; Vratsinis et al., 2025; Fang et al., 2026). We leverage this advantage to present, to our knowledge, the first power curve verification using motion-compensated nacelle-mounted wind lidar.

In Sect. 2.1, we describe the field campaign and the measurement configuration of the wind lidars and the data post-processing steps. In Sect. 3, we present a model that expresses the wind lidar measurements as a function of wind profile characteristics. This model is used to study the inflow conditions. Finally, in Sect. 4, we present our results on wind profile characteristics and their impact on the power production of the FOWT. The implications of these results are discussed in Sect. 5.

2 Material & Methods

2.1 Field Study

The wind turbine examined in this study is one of five floating offshore wind turbines (FOWTs) that form the Hywind Scotland wind farm. The FOWTs (SWT-6.0-154, Siemens Gamesa Renewable Energy) have a hub height of 98.6 m and a rotor diameter of D=154 m. They are mounted on floating platforms based on a ballasted spar buoy concept and have been operating since 2017 Jacobsen and Godvik (2021).

The most notable motion experienced by the wind turbines during operation occurs along the pitch axis, with angles ranging from 0° to 7° at wind speeds between cut-in and rated Angelou et al. (2023). Above the rated wind speed, the pitch angle decreases until it reaches a mean value close to 2°. Less significant variations are observed in the roll angle, which on average ranges between 0° and 0.5° for wind speeds between cut-in and rated. In contrast to the pitch angle, the roll angle continues to increase above rated speed, reaching approximately 1°. When comparing the magnitude of the mean pitch and roll angles, the roll angle is 60 – 90 % smaller than the pitch angle. In addition to the mean rotation about the pitch and roll axes, the operation of the Hywind Scotland turbines is characterised by wind-speed-dependent dynamic rotations around the yaw, pitch, and roll axes Jacobsen and Godvik (2021). The standard deviation of the yaw and roll angles follows a similar trend, increasing with hub-height wind speed and reaching a maximum of about 0.8° and 0.4°, respectively. By contrast, the maximum standard deviation of the pitch (i.e. 0.8°) occurs near the rated wind speed, while at lower and higher wind speeds the standard deviation

https://doi.org/10.5194/wes-2026-20
Preprint. Discussion started: 16 February 2026

eawe european academy of wind energy
Open Access WIND ENERGY SCIENCE DISCUSSIONS

of the pitch is less than 0.4°. Furthermore, the magnitude of the dynamic motion of the Hywind Scotland turbines depends on atmospheric stability, with lower dynamic motion in all yaw, pitch, and roll rotations observed under stable conditions. Overall, the observed mean and dynamic pitch motion indicates that the Hywind Scotland wind turbine tilts away from the wind in a stable manner, as the standard deviation of the pitch angle remains small. This is not necessarily the case for other floater types. For example, Gräfe et al. (2023) reports FOWT pitch angles with a lower mean magnitude but higher dynamic motion.

2.2 Wind Lidar

The inflow wind conditions experienced by the wind turbine were monitored using a nacelle-mounted Doppler lidar. The Doppler lidar (*Wind Iris Turbine Control*, Vaisala Oyj) acquires radial wind speed measurements along four separate lines of sight. The direction of each line of sight is defined by a three-dimensional unit vector $\mathbf{n} = \{n_1, n_2, n_3\}$, with azimuth angles of $-15°$ or $+15°$ and tilt angles of $-5°$ or $+5°$, relative to the instrument's optical axis (see Fig. 1). Radial wind speeds are acquired at ten distances from the lidar: 50 m ($0.32D$), 80 m ($0.52D$), 120 m ($0.78D$), 160 m ($1.04D$), 200 m ($1.30D$), 240 m ($1.56D$), 280 m ($1.82D$), 320 m ($2.08D$), 360 m ($2.34D$), and 400 m ($2.60D$), all distances measured along the optical axis of the Doppler lidar. The transceiver of the lidar was tilted by 2.5° relative to a levelled nacelle. Although the Wind Iris is a *fixed-pattern-scanning*[2] Doppler lidar, its installation on a FOWT caused the measurement geometry to be distorted by turbine motion. When the turbine tilt angle reaches 5°, corresponding to hub-height wind speeds between 8.5 – 9.5 m s^{-1} and 12.5 – 13.5 m s^{-1}, the lidar configuration consists of two beams that are nearly horizontal and two beams measuring across the upper part of the rotor (see Fig. 1(a)). In this configuration, the three furthest range gates of the lower beams and the four furthest range gates of the upper beams are located outside the rotor plane (see Fig. 1(b)).

2.3 Data

The wind turbine was instrumented with a motion reference unit (MRU) installed on the nacelle to monitor its mean and dynamic responses. The MRU measures the pitch and roll angles of the nacelle, corresponding to rotations about the longitudinal and transverse axes relative to the turbine's yaw direction. Data from the MRU were logged alongside active power and wind speed measurements from a nacelle-mounted anemometer via the supervisory control and data acquisition (SCADA) system at 1 Hz. Unlike the other parameters, the yaw direction was recorded only when changes occurred. Doppler lidar data were acquired at a frequency of 1 Hz per line of sight, meaning a complete set of radial wind speed observations for all lines of sight was available every four seconds. Synchronisation between the two data acquisition systems was verified by comparing the internal accelerometer readings of the Doppler lidar with those from the MRU in the nacelle.

In this study, we examine data from January 2019 to October 2020. The dataset does not cover the entire period but includes three intervals: 01/01/2019 – 30/01/2019, 01/09/2019 – 29/11/2019, and 01/06/2020 – 01/10/2020. Discontinuities were due either to missing turbine data or periods when the nacelle-mounted lidar was not operating. Overall, the dataset contains SCADA measurements equivalent to approximately six months.

[2]Definition according to IEC 61400-50-3 (2022)

https://doi.org/10.5194/wes-2026-20
Preprint. Discussion started: 16 February 2026

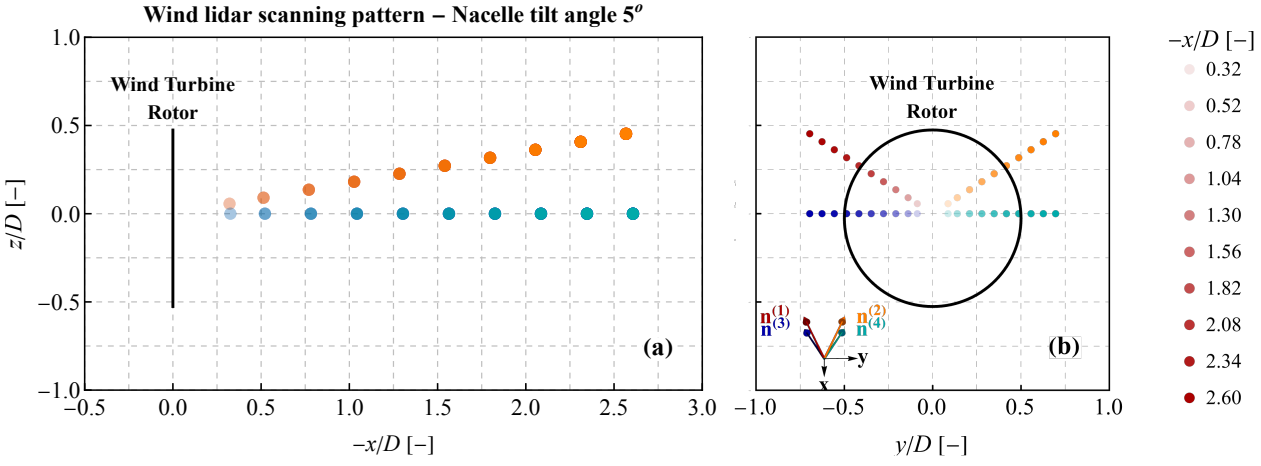

Figure 1. Scanning pattern of the nacelle-mounted wind lidar when the tilt of the floating offshore wind turbine was equal to 5°, corresponding to the wind speed ranges 8.5 – 9.5 ms^{-1} and 12.5 – 13.5 ms^{-1}. The two lower beams (denoted as $\mathbf{n}^{(3)}$ and $\mathbf{n}^{(4)}$) are almost horizontal when the pitch angle is approximately equal to 5°. The x-axis is parallel to the yaw direction and pointing downwind.

To avoid including periods when wakes from adjacent turbines distorted the inflow conditions of the HS4 turbine, only data acquired during turbine operation with yaw directions between 90° and 270° were selected. From the 13,247 ten-minute periods identified, lidar data were available for 6,729 periods. Additionally, some periods exhibited large yaw standard deviations. To focus on stable wind direction, only periods where the yaw standard deviation within a ten-minute interval was $\leq$10° were retained. Applying these criteria resulted in a dataset of 6,659 cases (i.e. ten-minute periods). The selected dataset represents climatological conditions typical of summer and autumn. The SCADA data were post-processing to estimate synchronized statistics with the wind lidar. The wind lidar data were processed using the instrument's quality index and by removing radial speed outliers per one-hour period, following the procedure described in Angelou et al. (2023).

3 Wind Profile Parametrization

To study the inflow conditions, we examine the mean radial wind speed across the four lines of sight and derive parameters describing the vertical profile at the upper part of the wind turbine rotor. For this purpose, we define first a three-dimensional coordinate system with its origin at the nacelle-mounted wind lidar and the x-axis aligned with the turbine's yaw direction and pointing downwind. Second, we consider that the wind vector U is described by three components: u, v and w. Subsequently,we assume that the inflow, undisturbed by the presence and operation of the wind turbine, is horizontally homogeneous, such that the wind vector $\mathbf{U}$ at a position with coordinates $\{x, y, z\}$ satisfies $U(x, y, z) = U(z)$. The inflow conditions are characterised by parameterising the vertical profile as a function of: i) the longitudinal $\overline{u}_\infty$ and transverse $\overline{v}_\infty$ mean components of the free

https://doi.org/10.5194/wes-2026-20
Preprint. Discussion started: 16 February 2026

eawe european academy of wind energy
Open Access WIND ENERGY SCIENCE DISCUSSIONS

wind vector $\mathbf{U}$ at the nacelle height (the overbar denotes mean quantities), and ii) the gradients of these components (i.e. $\frac{\partial \overline{u}}{\partial z}$ and $\frac{\partial \overline{v}}{\partial z}$).

Furthermore, we adopt the assumptions about free inflow described in Angelou et al. (2023), namely: i) the two horizontal mean wind components $\{\overline{u}, \overline{v}\}$ at a given height are horizontally homogeneous within each measurement distance; ii) the vertical wind component is negligible ($\overline{w} = 0$ ms^{-1}); and iii) the wind shear $\frac{\partial \overline{u}}{\partial z}$ and veer $\frac{\partial \overline{v}}{\partial z}$ within the vertical range of the nacelle-mounted lidar's measurement area are constant with height. Using these assumptions, and considering that the distortion of the inflow wind speed induced by turbine operation can be expressed as a function of an induction factor Medici et al. (2011); Simley et al. (2016), we express the line-of-sight measurements of the nacelle-mounted wind lidar as:

$$\begin{pmatrix} v_r^{(1)} \\ v_r^{(2)} \\ v_r^{(3)} \\ v_r^{(4)} \end{pmatrix} = -\boldsymbol{M} \begin{pmatrix} \overline{u}_\infty \\ \frac{\partial \overline{u}}{\partial z} \\ \overline{v}_\infty \\ \frac{\partial \overline{v}}{\partial z} \end{pmatrix} \quad \text{where} \quad \boldsymbol{M} = \begin{pmatrix} \vdots & & & \\ n_1^{(i)} f_{\text{ind}}(n_1^{(i)} d_f) & n_1^{(i)} n_3^{(i)} d_f f_{\text{ind}}(n_1^{(i)} d_f) & n_2^{(i)} & n_2^{(i)} n_3^{(i)} d_f \\ \vdots & & & \end{pmatrix} \tag{1}$$

is the matrix of the line-of-sight unit vectors and d_f is the distance from the instrument to the measurement volume. This parametrisation is commonly used to express nacelle-mounted wind lidar observations as a function of wind conditions Borraccino et al. (2017); Angelou et al. (2023). Each measurement in the *Wind Iris* dataset is tagged with the corresponding upwind distance x_f, reported as the nominal horizontal distance from the instrument along the x-axis. The actual distance d_f can be computed by multiplying x_f by the norm of the vector $\{1, \tan\phi, \tan\theta\}$, where ϕ and θ correspond to the azimuth and elevation angles of the lines of sight, respectively. The reduction of longitudinal wind speed along a line normal to the rotor centre, as described by vortex sheet theory (Conway, 1995; Medici et al., 2011), is expressed by the induction factor a. This factor adequately describes the evolution of wind speed as it approaches a turbine rotor, as demonstrated in a field test by Simley et al. (2016) for an onshore wind turbine, using the following formula:

$$\frac{\overline{u}}{\overline{u}_\infty} = 1 - a\left(1 + \frac{\zeta}{\sqrt{1+\zeta^2}}\right), \tag{2}$$

where $\zeta = -x/R$ is the distance normalized by the rotor radius $R = 77$ m and a is the induction factor. The model is applied to all measurements, including the furthest range gates located outside the rotor plane. The estimation of the induction factor remains unchanged even when considering its radial distribution, for example by using the empirical model of Troldborg and Meyer Forsting (2017). The performance of the model in estimating upwind mean wind speed characteristics is assessed by calculating the root-mean-square error (hereafter denoted as ε_u) between the modelled and measured radial wind speeds for each 10-minute period.

https://doi.org/10.5194/wes-2026-20
Preprint. Discussion started: 16 February 2026

eawe european academy of wind energy
Open Access WIND ENERGY SCIENCE DISCUSSIONS

3.1 Vertical wind profile

Based on the radial speed measurements acquired at the same height but from different lines-of-sight, it is possible to estimate the longitudinal and transverse components of the wind vector. For this calculation, an estimation of the induction factor a of the wind turbine is required. The two horizontal wind components are then equal to:

$$u(z) = \frac{n_2^{(j)} v_r^{(i)} - n_2^{(i)} v_r^{(j)}}{f_{\mathrm{ind}}(n_1 d_f)(-n_1^{(j)} n_2^{(i)} + n_1^{(i)} n_2^{(j)})} \quad \text{and} \quad v(z) = \frac{-n_1^{(j)} v_r^{(i)} + n_1^{(i)} v_r^{(j)}}{-n_1^{(j)} n_2^{(i)} + n_1^{(i)} n_2^{(j)}}, \tag{3}$$

where the superscripts i and j denotes the index of the line-of-sight. Using Eq. 3 it is possible to reconstruct a wind profile at the top part of the rotor.

4 Results

4.1 Modelling the radial speed of the Doppler lidar

The first objective of this study is to assess how well the radial speed model presented in Eq. 1 reproduces the trends observed in the lidar data. In parallel, the study aims to identify cases where the model disagrees with the observations and investigate which assumptions about the wind conditions were inadequate.

Figure 2 shows the mean radial speeds for each line of sight during four separate 10-minute periods, all characterised by the same hub-height wind speed (8 m s^{-1}). Each case represents different inflow conditions and corresponds to periods where lidar measurements were available for all 10 range gates along each line of sight. Figure,2(a) illustrates the simplest wind conditions: a positive shear ($\frac{\partial \overline{u}}{\partial z} > 0$) and negligible veer ($\frac{\partial \overline{v}}{\partial z} \sim 0$). The radial speed model (solid lines), based on constant shear and veer assumptions, adequately describes the observations (dots). When the turbine yaw is aligned with the wind direction, the two lower beams measure the same line of sight at any distance. Vertical shear results in higher radial speeds for the upper beams compared to the lower beams, while vertical veer causes larger deviations in the upper beams because wind direction changes with height. This effect is evident in Fig;2(b), where shear and veer cause the wind direction to change by 18° between hub height and blade tip height. Agreement between observations and the radial speed model is not limited to cases of positive shear and veer; it is also found in cases of negative shear. An example is shown in Fig;2(c), where negative shear at the top of the rotor results in lower radial speeds for the upper beams compared to the lower ones. Even when shear is zero, differences between upper and lower beams are expected due to the tilt angle affecting the projection of the horizontal wind vector on the upper beam's line of sight, typically resulting in a 1.5% – 2.5% difference. However, the observed differences range from 5% to 20%, depending on the upper beam and measurement range, which indicate the presence of negative shear. In all three cases, a clear reduction in radial wind speed is observed around 160 m ($\sim 1D$) towards the rotor, caused by turbine operation. This reduction corresponds to high induction factors (0.38 – 0.41), consistent with velocity deficits in the wake when the turbine operates below rated wind speed Angelou et al. (2023). Similar high induction factors have been reported by Larsen and Hansen (2014), who investigated aerodynamic induction of a full-scale wind turbine using two scanning Doppler lidars.

https://doi.org/10.5194/wes-2026-20
Preprint. Discussion started: 16 February 2026

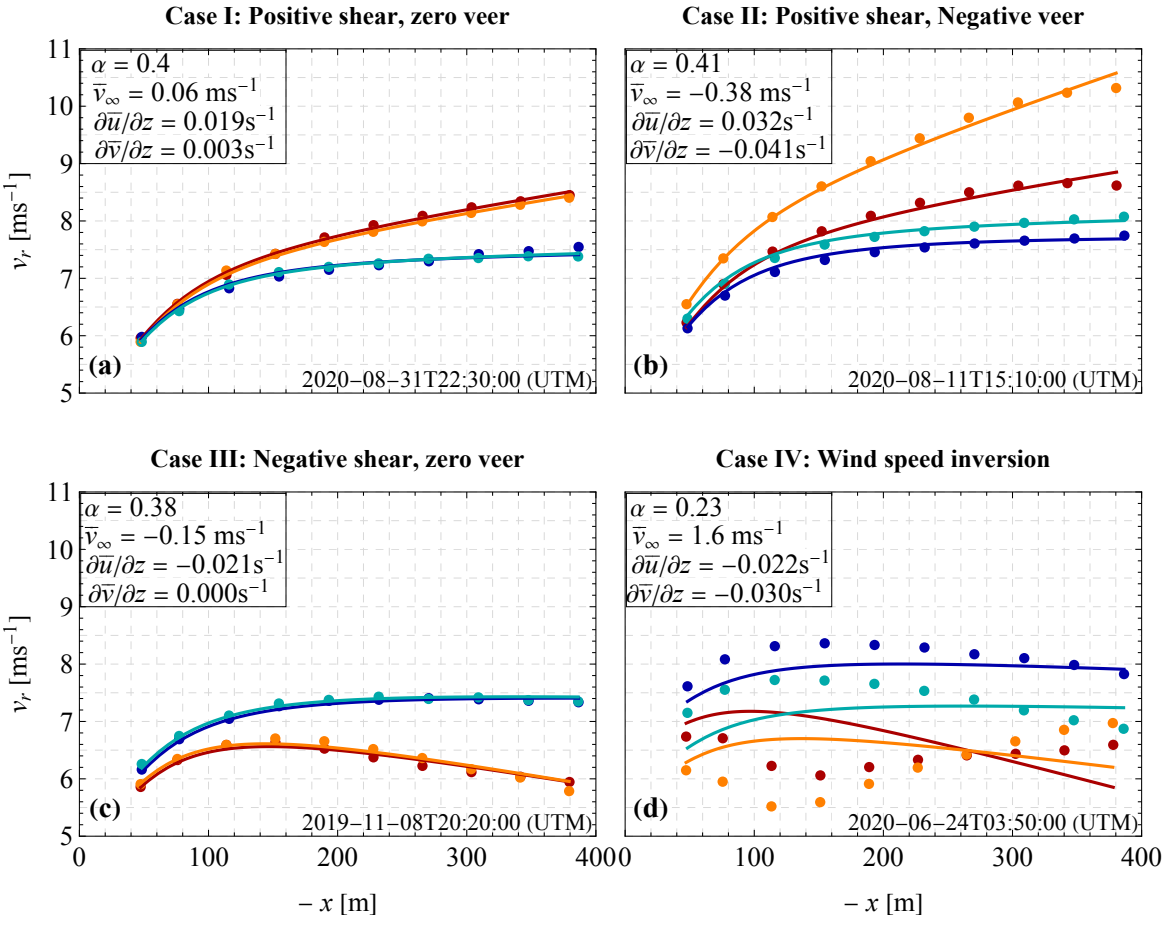

Figure 2. Example of the mean radial speed measurements of a nacelle-mounted wind lidar acquired over four different line-of-sights (i.e. $n^{(i)}$, with i=1,2,3 and 4) and upwind distances (i.e. 50 – 400 m) during 10-minute periods when the wind profile was characterized by positive shear and zero veer (a), positive shear and negative veer (b), negative shear and zero veer (c) and by wind speed inversion (d). The information of the upwind conditions ($\bar{v}_\infty$, $\frac{\partial \bar{u}}{\partial z}$ and $\frac{\partial \bar{v}}{\partial z}$) and the induction factor a of the wind turbine of each example is presented the corresponding plot.

In contrast to the good agreement observed in Fig.,2(a) –(c), which corresponded to cases where the RMSE of Eq. 1 has values less than 0.2 m s^{-1}, 11% of the examined 10-minute periods show that the inflow model could not reproduce the trends in the lidar data (see Fig. 2(d)). This discrepancy is attributed to wind profiles with wind speed inversions, as occurs in low-level jets (LLJs). In such cases, simplified parameterisations of the vertical wind profile (i.e. constant shear and veer coefficients) cannot predict the observed radial speed distribution. Consequently, the root mean square error between the model in Eq.,1 and the observations exceeds 0.2 m s^{-1}, the empirically selected threshold used to distinguish cases where inflow assumptions are adequate.

https://doi.org/10.5194/wes-2026-20
Preprint. Discussion started: 16 February 2026

eawe european academy of wind energy
Open Access WIND ENERGY SCIENCE DISCUSSIONS

4.2 Wind profile characteristics

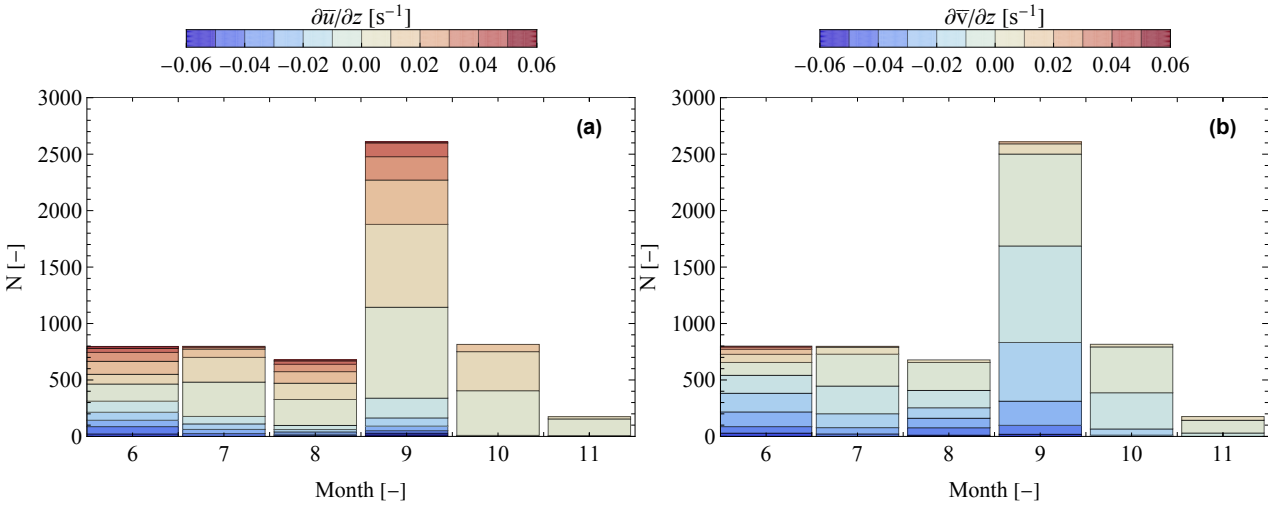

Figure 3. Bar chart of the distribution of the estimated wind shear $\frac{\partial \overline{u}}{\partial z}$ and veer $\frac{\partial \overline{v}}{\partial z}$ for different 10-minute periods over different months.

The analysis of wind profile characteristics was conducted only for 10-minute periods where the model in Eq. 1 performed adequately. These cases were identified by inspecting the root mean square error (RMSE) between the inflow model and the 10-minute mean radial speeds. Values above 0.2 m $^{-1}$ were considered unsatisfactory for representing the spatial distribution of the lidar measurements. This threshold was empirically chosen and corresponds to mean absolute differences of less than 5% between hub-height wind speed measurements from the nacelle-mounted lidar and the turbine anemometer Angelou et al. (2023). As already stated in the previous section, based on this criterion, 757 cases (11% of the dataset) were excluded. As shown in Fig. 2(d), these cases are likely associated with the presence of low-level jets (LLJs). A similar occurrence of LLJs (approximately 12%) during spring and summer months by in an offshore field campaign in the North Sea Kalverla et al. (2017). During these events, the turbine yaw direction covered a sector from 90° to 256°, indicating that LLJs cannot be solely attributed to wind flowing over a coastal–sea interface.

Figure 3 presents a bar chart of the estimated wind shear and veer for each month. The wind shear within the height layer where the top part of the FOWT is found range from -0.06 s^{-1} to 0.06 s^{-1} (Fig. 3(a)). This shows the large variability of the wind profile that the wind turbine interacts with. Periods with negative shear are found during the months from June to September and account for 22% of the dataset, a percentage similar to that reported by Furevik and Haakenstad (2012), who studied wind profile characteristics over the North Sea. Such profiles, which may include LLJs, typically occur in areas with variations in topography Tuononen et al. (2015). For negative shear cases, it remains unclear whether the core of a LLJ is found within the lower half of the rotor or if a wind speed inversion occurs at very low heights, as observed in the North Sea Furevik and Haakenstad (2012). When focusing on data acquired between June and September, negative shear does not consistently occur when the wind originates from a specific sector. Only during July and September, negative shear is observed in a narrow

https://doi.org/10.5194/wes-2026-20
Preprint. Discussion started: 16 February 2026

eawe european academy of wind energy
Open Access WIND ENERGY SCIENCE DISCUSSIONS

wind direction sector between 200° and 250°. These values appear in at least one 1-hour period on 13 days in July and almost every day (i.e. 30 days) in September. In contrast, during June and August, negative shear is not associated with a specific wind direction sector but occurs across the entire selected sector (90° – 270°), as shown in Appendix A. The observed negative shear values are independent of the time of day. The vertical gradient of the transverse wind component is generally found negative, as expected in the location of the FOWT (Fig. 3(b)), with the higher values been observed in cases when the wind shear is strong.

4.3 Low-level jets

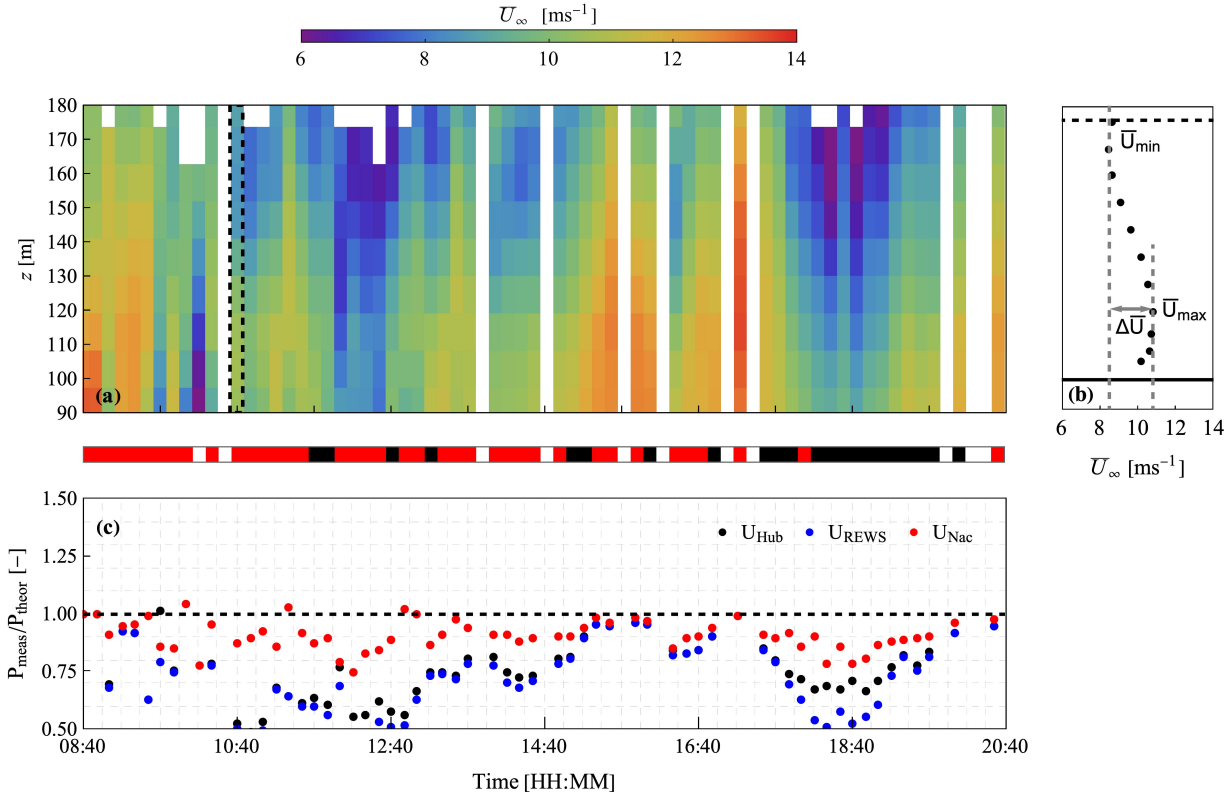

Figure 4. Case study of a 12-h period when the vertical wind profiles are characterized by negative shear and wind speed inversions. The time series of the vertical profile of the horizontal free wind speed (U_∞) is presented in (a). An example of one of the profiles where a wind speed inversion is observed, highlighted by a dashed rectangle in (a), is shown in (b). The characterization of each profile is visualised using black (case of negative shear), red (wind speed inversion) and white (cases of positive shear or data that is missing) in a bar below the density plot (a). The power produced by the wind turbine, normalized by the nominal value based on the power curve is presented in (c) using either the hub height wind speed estimated using the wind lidar (U_{Hub}) or the sonic anemometer (U_{Hub}) installed on the nacelle or the rotor equivalent wind speed (U_{REWS}).

https://doi.org/10.5194/wes-2026-20
Preprint. Discussion started: 16 February 2026

eawe european academy of wind energy
Open Access WIND ENERGY SCIENCE DISCUSSIONS

To further investigate wind profiles with negative shear and/or wind speed inversions, we examine a 12-hour period between 08:40 and 20:40 on 26-06-2020. Figure 4(a) shows the corresponding wind conditions. The figure presents the mean horizontal wind speed U_∞ at different heights, corresponding to the magnitude of the two horizontal components (i.e. $\sqrt{\overline{u}_\infty + \overline{v}_\infty}$), which are calculated using Eq. 3. The estimation of these components is based on pairs of radial speed measurements acquired at different ranges and heights, and represents the spatial average over 10-m vertical layers. This period was chosen because it is characterised by vertical profiles with either negative shear or a speed inversion (highlighted in red or black, respectively, in the bar below Fig. 4(a)).

In the cases of negative shear, the wind speed decreases from hub height (98.6 m) towards the top of the rotor (∼170 m) at rates varying between 0 s^{-1} and -0.05 s^{-1}. On these occasions, a speed inversion occurs somewhere below hub height, but due to the absence of measurements in the lower half of the rotor, its exact location cannot be determined. For wind profiles with a speed inversion, the profiles typically exhibit one inflection point around a maximum value. In a few cases, profiles such as that shown in Fig. 4(b) display two inflection points, around a maximum and a minimum, within the vertical range of 90 – 180 m, that form a *core* in the wind profile. The presence of two inflection points enables identification of LLJs based on the difference ($\Delta\overline{U}$) between the minimum ($\overline{U}_{\min}$) and maximum ($\overline{U}_{\max}$) wind speeds. In addition to these vertical profile features, this period is noteworthy for its highly variable hub-height wind speed, ranging from 6 m s^{-1} to 14 m s^{-1}, with a yaw direction between 140° and 180°. This makes it an interesting case for studying turbine power production under different inflow conditions. Figure 4(c) shows the turbine power output normalised by the nominal value based on the power curve corresponding to hub-height wind speed, using either the wind lidar (U_{Hub}) or the sonic anemometer (U_{Nac}) installed on the nacelle. Deviations from nominal power reach up to 50%, with smaller deviations observed when using the nacelle-mounted sonic anemometer as the reference wind speed. These results indicate that inflow conditions with negative shear or speed inversions can significantly impact FOWT power production. Therefore, it is important to quantify the height at which wind speed inversions occur, the magnitude of the associated speed difference, and the duration of these events. Figure 5 presents the duration, inversion height, and wind speed difference between the maximum and minimum wind speeds within the examined height range (100 – 200 m). Most profiles persist for about 60 minutes; however, eight periods were identified where these characteristics lasted for an extended duration (700 – 900 minutes). Roots et al. (2025) reported similar LLJ duration statistics. For a slight majority of cases, the inversion height was around 130 m, but overall, the range was 100 – 160 m. The wind speed difference was usually small (0.25 – 0.5 m s^{-1}), although in 10% of cases differences greater than 2 m s^{-1} were observed.

4.4 Power curve verification

The transceiver of the nacelle-mounted wind lidar was installed approximately 4.5 m above the rotor centre. Consequently, Eq. 1 estimates the two components of the horizontal free wind vector at a position vertically displaced relative to hub height. To verify the installation height of the wind lidar (z_L), we calculated the mean minimum absolute difference between the hub-height wind speed reported by the nacelle-mounted anemometer and a wind speed estimated using the function $\overline{u}_\infty + \dfrac{\partial \overline{u}}{\partial z} z_L$. Different values of z_L were tested for all periods, ranging from -10 m to 10 m in steps of 0.1 m, and the minimum difference

https://doi.org/10.5194/wes-2026-20
Preprint. Discussion started: 16 February 2026

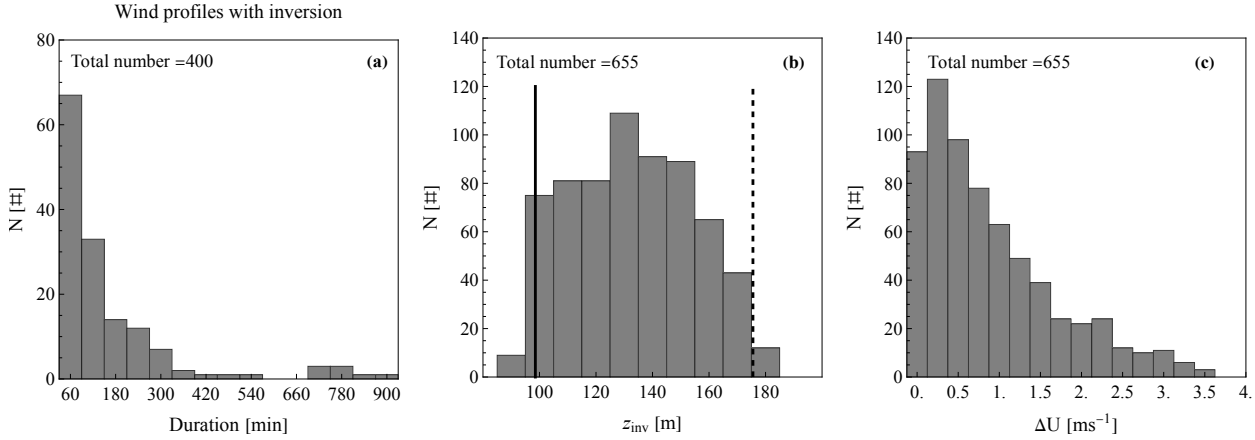

Figure 5. Duration, the height of the wind speed inversion (z_{inv}) and the wind speed difference (ΔU) between the maximum and the minimum wind speed along the wind vertical profile.

was found when the lidar was translated vertically by 4 m. This height offset is therefore used to estimate hub-height wind speed.

In the case presented in Fig. 4, vertical wind profiles with speed inversions or negative shear at the top of the rotor lead to a reduction in turbine power production (as a reference, we used the power curve of a bottom-fixed turbine of the same type as the FOWT examined in this study). To assess the impact of inflow conditions on FOWT power production, we performed a power curve verification (PCV) analysis. For this purpose, an accurate hub-height wind speed estimate is required. Although the lower beams are nearly horizontal at a 5° turbine pitch, the mean turbine angle places them between approximately 60 m and 125 m (see Appendix B). Therefore, we examine three hub-height wind speed estimation methods that can be used in the context of a PCV:

1. Wind Field Reconstruction (2.6 D): The hub-height wind speed is calculated using Eq.,1 with measurements only at 2.6 D (see Fig. 6(a)). Note that the nacelle pitch angle causes the measurement plane at a given distance to be tilted rather than vertical. The tilt is proportional to the nacelle pitch. However, because nacelle-mounted lidars typically use low elevation angles for their lines of sight, this tilt has minimal impact on the horizontal distance from the rotor. Considering that measurements are acquired over a probe length, the horizontal displacement can be treated as negligible.

2. Wind Field Reconstruction (All Range Gates): The hub-height wind speed is calculated using Eq. 1 with all available measurements (see Fig. 6(b)).

3. Rotor Equivalent Wind Speed (REWS): The hub-height wind speed is estimated using the REWS as defined in IEC 61400-12-1 (2022). For this calculation, we assume that the wind shear estimated at the top of the rotor is representative of conditions at the bottom. Due to this assumption, REWS is calculated only for cases where positive shear is estimated

https://doi.org/10.5194/wes-2026-20
Preprint. Discussion started: 16 February 2026

using Eq. 1. For profiles with negative shear, the location of wind speed inversion in the lower rotor cannot be determined, so using the estimated parameters to compute REWS is not justified.

The purpose of testing the three wind speed estimates is to investigate how sensitive the power curve verification is to the choice of reference wind speed. Both the mean (Figs. 6(a) – (c)) and the standard deviation (Figs. 6(d) – (f)) of the produced power are evaluated. We observe a notable difference in the power curve between positive and negative wind shear conditions (Figs. 6(a) – (b)). The estimation of REWS, shown in Fig. 6(c), results in a power curve similar to those obtained using the other two hub-height wind speed definitions. Typically, using REWS reduces scatter in the power curve depending on the magnitude of wind shear Wagner et al. (2011). For low wind shear values, only small differences are observed when REWS is applied Wagner et al. (2014a); Van Sark et al. (2019). In our dataset, offshore wind conditions produce power curve scatter, expressed by the standard deviation of power, that is comparable across all three hub-height wind speed estimates. However, a significant difference is observed in the case of negative shear profiles, where the standard deviation is nearly twice that of positive shear cases below rated speed.

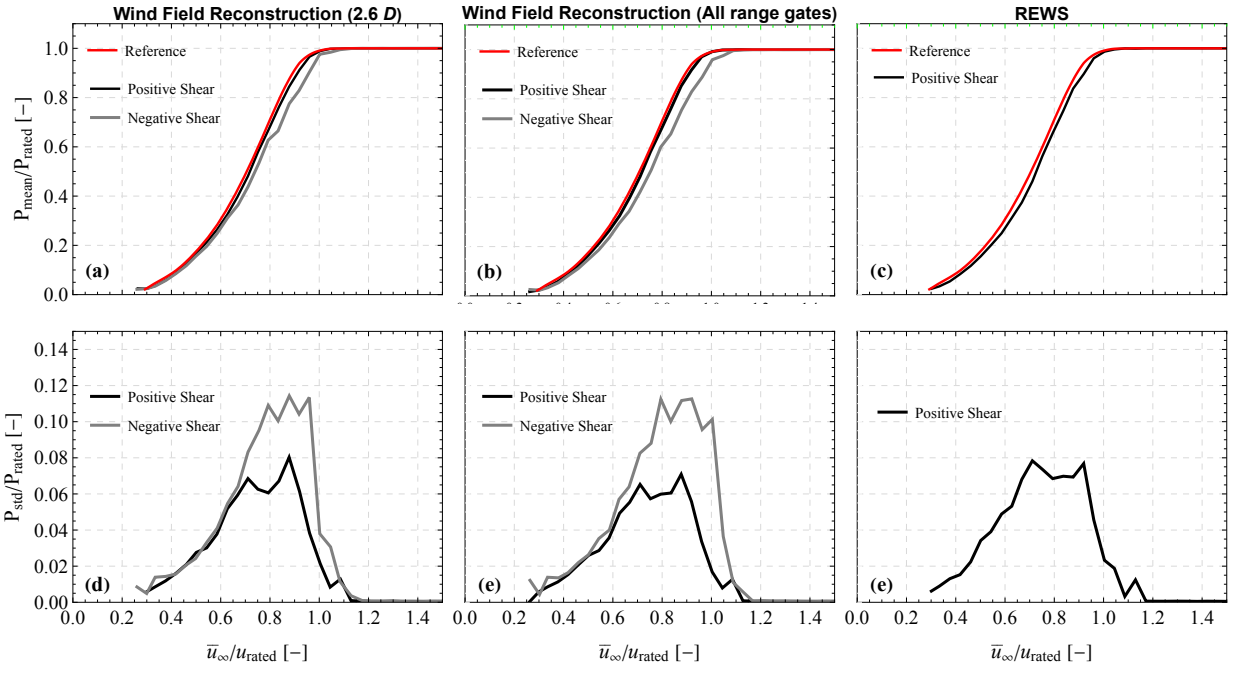

Figure 6. Normalized power produced by turbine HS4 at Hywind Scotland versus (a) the wind speed measurements from the nacelle-mounted anemometer, (b) the hub-height wind speed estimated using the nacelle-mounted wind lidar and (c) the REWS.

To quantify the variations between the estimated power curve and the reference curve, we calculate the relative difference using three different wind speed estimates. Figure 7 shows the relative difference between cases with negative and positive shear and the reference power curve. The differences observed in Fig. 6 are quantified by calculating the relative percentage

https://doi.org/10.5194/wes-2026-20
Preprint. Discussion started: 16 February 2026

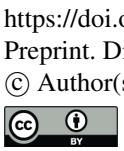

eawe european academy of wind energy
Open Access WIND ENERGY SCIENCE DISCUSSIONS

difference between the measured and modelled power curves. We find that when the wind profile exhibits negative shear, power production is reduced by up to 18%. Smaller differences are observed in cases with positive shear. Interestingly, the difference between positive and negative shear ranges from 5% to 10%, depending on whether all range gates are used or only measurements at $2.5D$ are selected.

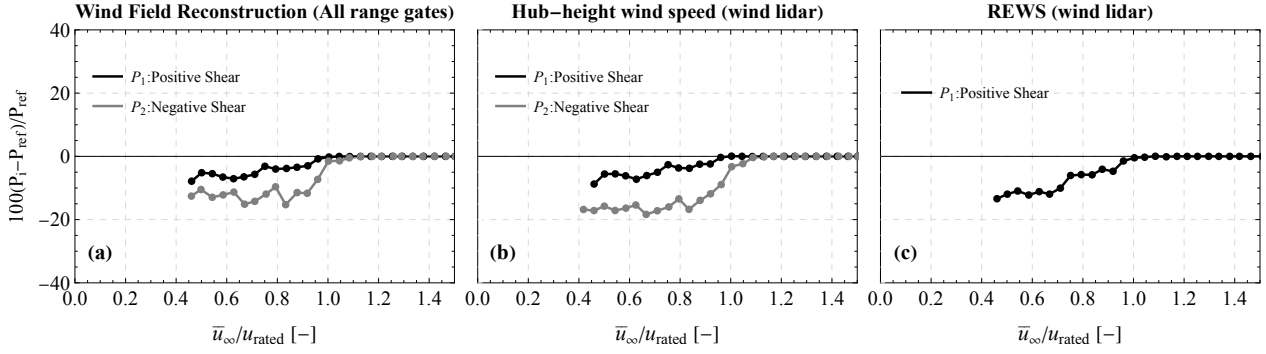

Figure 7. Relative difference between the estimated and the reference power curve versus: the hub-height wind speed calculated using either (a) all the radial wind speed measurements or (b) only the measurements at 2.6 D and (c) the REWS. In the plots (a) and (b) data from both negative and positive shears are used, while in the case of the REWS (c) only cases with positive shear.

5 Discussion

Two main limitations are identified in this study, which are related to sample size and available meteorological data. First, the characterisation of the wind profile was based on observations acquired between June and November. Therefore, it is not possible to determine whether the derived statistical distributions of shear (Fig. 3) and LLJ features (Fig. 5) are representative throughout the year or follow a specific seasonality. Second, measurements of the vertical gradient of atmospheric temperature were not available during the field campaign. Consequently, it is not possible to assess the stratification of the probed atmospheric layer, preventing classification of the data by atmospheric stability, a step that would enable a more detailed characterisation of inflow wind conditions.

The inflow conditions are parameterised assuming a simplified vertical distribution of wind speed. Using this parametrisation, we estimate hub-height wind speed for power performance verification of the wind turbine. If the turbine response is approximated as a beam, variations in pitch and roll angles can be used to estimate horizontal translation of the nacelle along the longitudinal and transverse axes relative to the yaw direction. Considering these variations, we find that the standard deviation of the transverse and longitudinal nacelle speeds are less than 0.2 m s^{-1}. These values introduce an uncertainty in hub-height wind speed estimation Gräfe et al. (2023). However, due to their small magnitude, they are not considered for the case of the FOWT examined in this study.

https://doi.org/10.5194/wes-2026-20
Preprint. Discussion started: 16 February 2026

The increasing size of offshore wind turbines can lead, as observed, to situations where wind field characteristics vary significantly along the rotor span (e.g. vertical profiles with inversions). We show that this can strongly affect turbine operation and the accuracy of power performance analysis. Therefore, measurements of wind shear and veer at as many heights as possible, and subsequent parametrisation of wind profiles, including negative shear or LLJs are essential for power curve verification. In such cases, it is beneficial to use multiple measurements covering both the top and bottom of the rotor, typically provided by commercial continuous-wave lidars, or, for pulsed lidars, to include more range gates. However, the latter requires incorporating line-of-sight measurements within the induction zone of the turbine into the parametrisation.

Currently, the requirements for wind turbine power verification are described in IEC 61400-12-1 IEC 61400-12-1 (2022). However, these standards apply to turbines installed over flat or complex terrain and do not account for the impact of turbine motion on power production or wind sensor accuracy. Furthermore, they do not consider cases where the wind profile deviates from the logarithmic law, which, as shown in this study, occurs frequently. For example, FOWT motion affects dynamic power variation and increases uncertainty in power production. Therefore, a revision of the standards is necessary. Measurements from nacelle-mounted lidars have been incorporated into standardised PCV procedures since the publication of IEC 61400-50-3 IEC 61400-50-3 (2022). These guidelines aim to be independent of lidar technology and apply to both flat onshore and offshore sites. Corrections for induction are not required by the standard. The recommended installation procedure for nacelle-mounted lidars includes pre-tilting the lidar to account for tower bending during turbine operation. However, nacelle-mounted lidars with multiple beams often lack measurements at hub height. In this study, the nacelle-mounted lidar was pre-tilted by 2.5° so that the two lower beams were nearly horizontal when the nacelle tilt was 5°. Levelled lines of sight are particularly useful for studying turbulence intensity in inflow conditions Peña et al. (2017); Mikkelsen et al. (2020); Peña et al. (2024) and can thus provide a useful input in power curve verification.

6 Conclusions

This study demonstrates that floating offshore wind turbines in deep-water environments are frequently exposed to complex atmospheric conditions, including negative wind shear and wind speed inversions within the rotor-swept area. These phenomena occurred in 22% and 11% of the examined cases, respectively and significantly influenced turbine power production, in respect to the corresponding power curve of a fixed-bottom wind turbine, particularly under negative shear. This is demonstrated in the case of 6 MW utility scale floating offshore wind turbine, that experiences mainly a wind-speed dependent pitch motion during operation. Our findings confirm that nacelle-mounted wind lidars are an effective tool for detecting such inflow characteristics, providing critical insights for improving power performance assessment and operational strategies for FOWTs.

Code availability. The post-processing, filtering, and analysis of the data were performed using the software system Wolfram Mathematica. For more information regarding the code used please contact Nikolas Angelou at nang@dtu.dk.

https://doi.org/10.5194/wes-2026-20
Preprint. Discussion started: 16 February 2026

eawe european academy of wind energy
Open Access WIND ENERGY SCIENCE DISCUSSIONS

Data availability. The data used in this study were acquired by Hywind Scotland. Hywind Scotland gave permission to DTU to analyze the data and publish the corresponding research findings. Due to a confidentiality agreement the data used in this study are not publicly available.

Appendix A: Climatology: Wind shear and veer

Figures A1 and A1 present scatter plots of the wind shear (sub-figures: a, c and e) and veer (sub-figures b, d and f) versus wind direction for the months June – August and September – November, respectively. The data correspond to 10-minute mean values. The wind direction correspond to the yaw direction of the HS4 wind turbine of the Hywind Scotland wind farm. The colour of each data point correspond to the root mean square error of Eq. 1. In the plots we can see that all months (except November) contain measurements from all different directions spanning from 180° to 360°. Estimations of large negative shear values are usually associated with high root mean square error values (i.e. $\epsilon_u > 0.2\text{m s}^{-1}$.) which corresponds to cases where the observed trends in the radial wind speed measurements cannot be reproduced by the model of Eq. 1.

https://doi.org/10.5194/wes-2026-20
Preprint. Discussion started: 16 February 2026

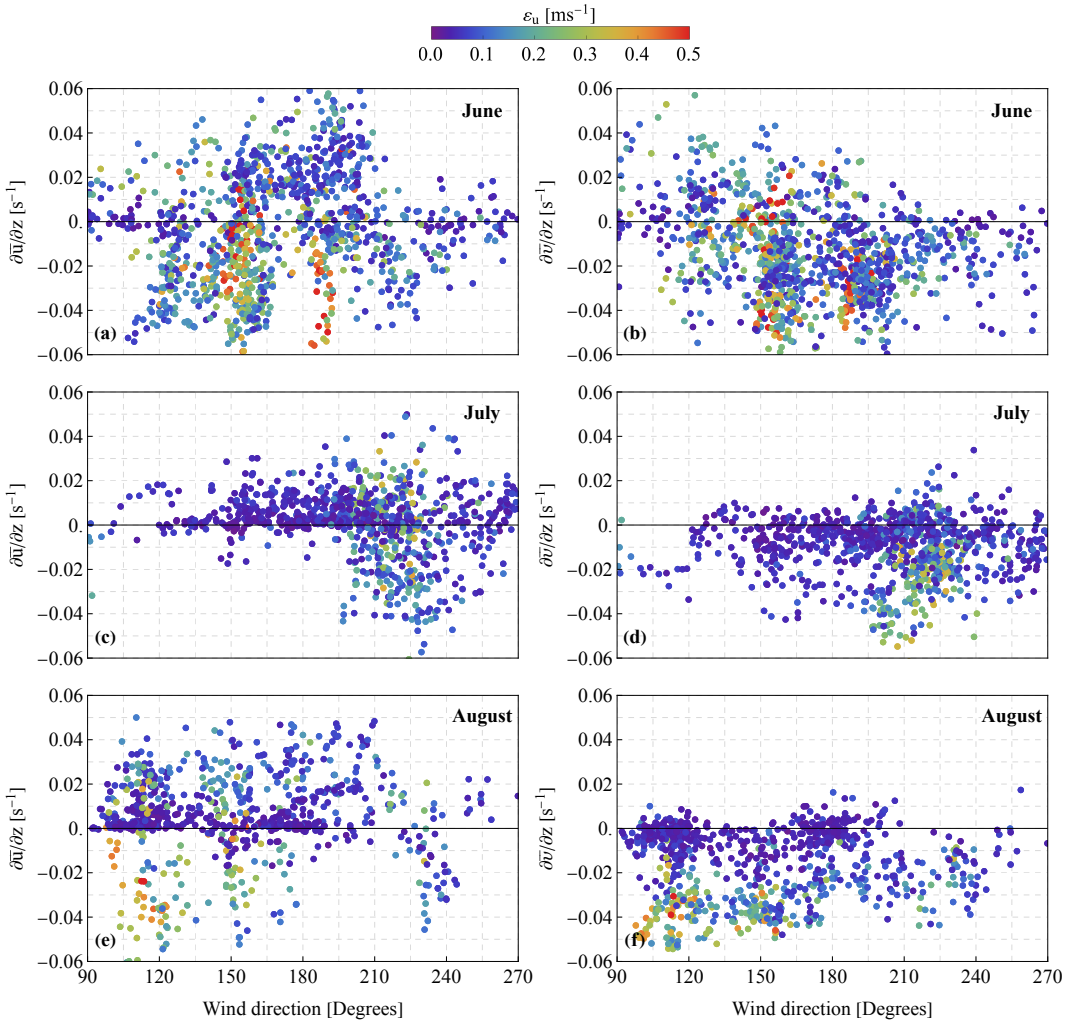

Figure A1. Shear and veer values for different 10-minute periods versus wind direction for the months June ((a) – (b)), July ((c) – (d)) and August ((e) – (f)).

https://doi.org/10.5194/wes-2026-20
Preprint. Discussion started: 16 February 2026

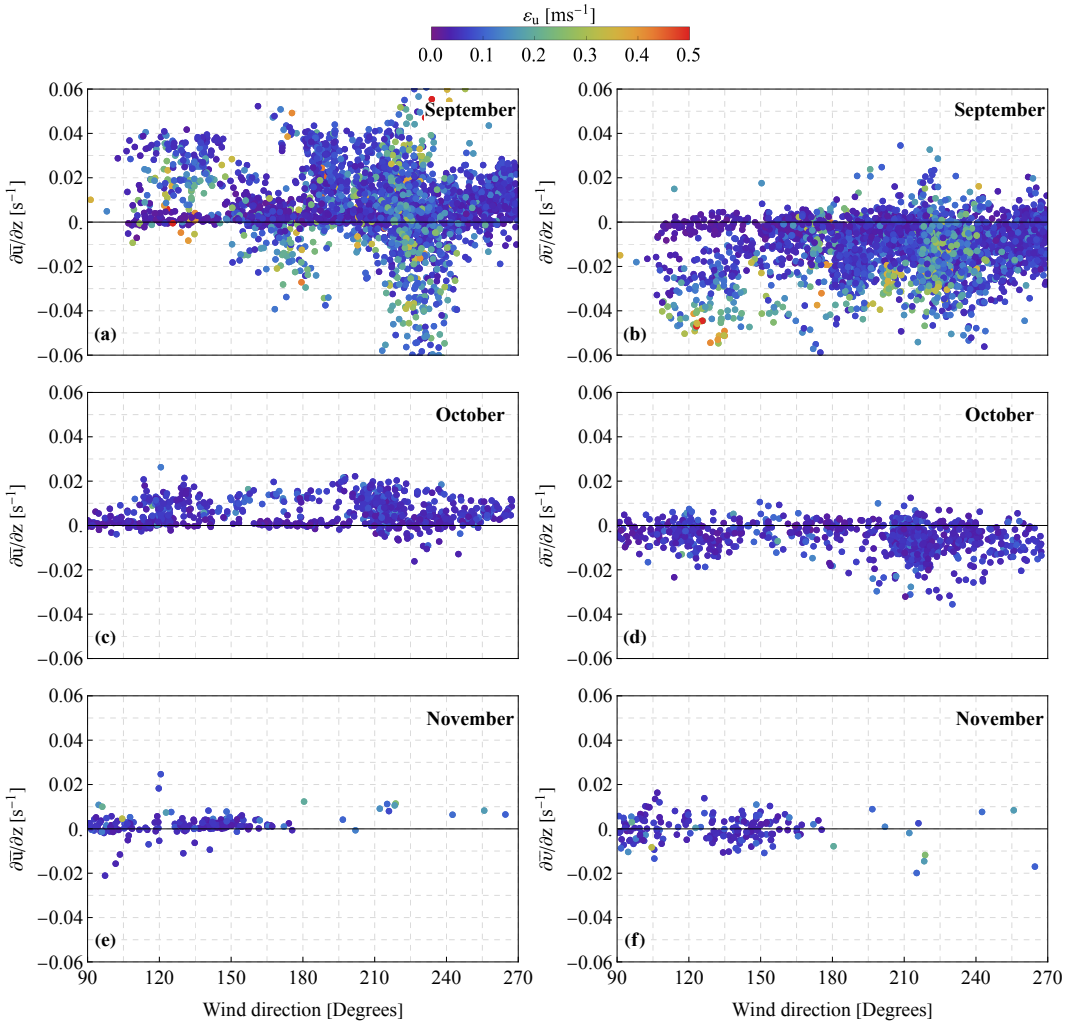

Figure A2. Shear and veer values for different 10-minute periods versus wind direction for the months September ((a) – (b)), October ((c) – (d)) and November ((e) – (f)).

https://doi.org/10.5194/wes-2026-20
Preprint. Discussion started: 16 February 2026

eawe european academy of wind energy
Open Access WIND ENERGY SCIENCE DISCUSSIONS

Appendix B: Height of the lower beams

The wind-speed dependent of the mean pitch angle of the wind turbine nacelle results in variations of the height of the two lower beams. Figure B1 the height of the two lower beams at the range gate of 2.6 D. These variations have not necessarily the same magnitude in the left Fig. B1(a) and right Fig. B1(b) line-of-sight measurements due to the mean roll angle of the nacelle.

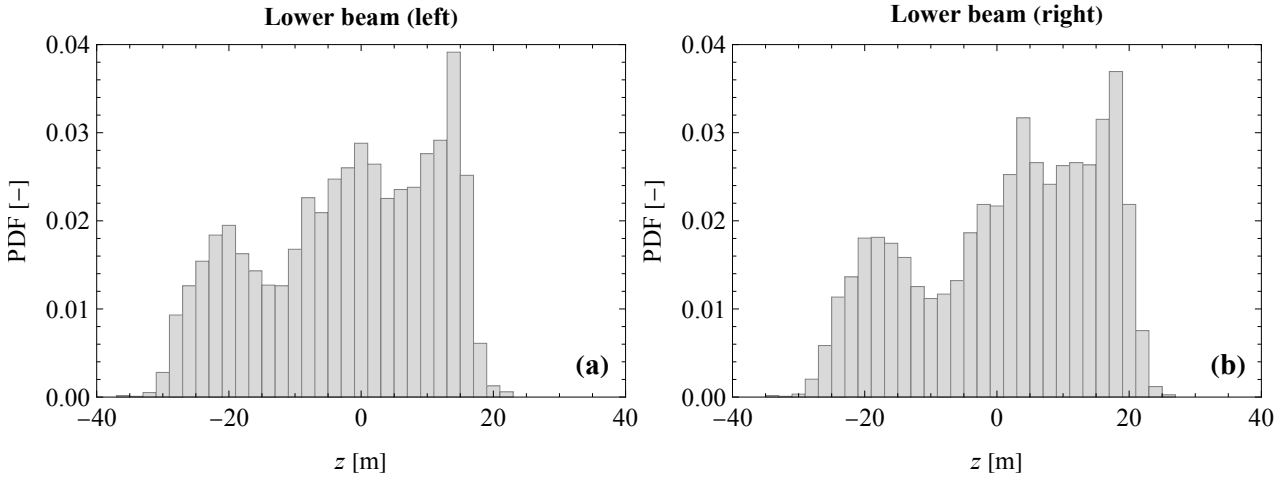

Figure B1. Probability density function of the height z of the range gate measurement of 2.6 D of the left (a) and right (b) lower beams of the nacelle-mounted Doppler lidar in relation to the hub-height.

Author contributions. The Hywind Scotland wind farm and CDB planned the campaign and performed the measurements; Conceptualization: NA and CDB, Data curation: NA, Formal analysis: NA, Investigation: NA, Methodology: NA and CDB, Validation: NA, Visualization: NA, Writing - original draft: NA, Writing & review editing: NA and CDB

Competing interests. The authors declare that they have no known competing financial interests or personal relationships that could have appeared to influence the work reported in this paper.

Acknowledgements. Hywind Scotland is acknowledged for providing access to the data. Michael Courtney, Head of the Section *Turbine Measurements* in the Department of *Wind and Energy Systems* of DTU is acknowledged for helping with the interpretation of the results of the power curve analysis. This research did not receive any specific grant from funding agencies in the public, commercial, or not-for-profit sectors.

https://doi.org/10.5194/wes-2026-20
Preprint. Discussion started: 16 February 2026

eawe european academy of wind energy
Open Access WIND ENERGY SCIENCE DISCUSSIONS

References

Angelou, N., Mann, J., and Dubreuil-Boisclair, C.: Revealing inflow and wake conditions of a 6 MW floating turbine, Wind Energy Science, 8, 1511–1531, https://doi.org/10.5194/wes-8-1511-2023, 2023.

Borraccino, A., Schlipf, D., Haizmann, F., and Wagner, R.: Wind field reconstruction from nacelle-mounted lidar short-range measurements, Wind Energy Science, 2, 269–283, https://doi.org/10.5194/wes-2-269-2017, 2017.

Bui, H., Bakhoday-Paskyabi, M., and Reuder, J.: Characterization and Bias-Correction of Low-Level Jets at FINO1 Using LiDAR Observations and Reanalysis Data, Wind Energy Science, https://doi.org/10.5194/wes-2025-91, 2025.

Conway, J. T.: Analytical solutions for the actuator disk with variable radial distribution of load, Journal of Fluid Mechanics, 297, 327–355, https://doi.org/10.1017/S0022112095003120, 1995.

Couto, A., Justino, P., Simões, T., and Estanqueiro, A.: Impact of the wave/wind induced oscillations on the power performance of the WindFloat wind turbine, Journal of Physics: Conference Series, 2362, 012 010, https://doi.org/10.1088/1742-6596/2362/1/012010, 2022.

Debnath, M., Doubrawa, P., Optis, M., Hawbecker, P., and Bodini, N.: Extreme wind shear events in US offshore wind energy areas and the role of induced stratification, Wind Energy Science, 6, 1043–1059, https://doi.org/10.5194/wes-6-1043-2021, 2021.

Doosttalab, A., Siguenza-Alvarado, D., Pulletikurthi, V., Jin, Y., Bocanegra Evans, H., Chamorro, L. P., and Castillo, L.: Interaction of low-level jets with wind turbines: On the basic mechanisms for enhanced performance, Journal of Renewable and Sustainable Energy, 12, https://doi.org/10.1063/5.0017230, 2020.

Fang, Y., Li, C., Liu, L., Guo, F., and Gao, Z.: Identification of wind inflow characteristics from nacelle lidar measurements in the induction zone of a 9 MW wind turbine, Renewable Energy, 256, https://doi.org/10.1016/j.renene.2025.124523, 2026.

FINO: Forschungsplattformen in Nord- und Ostsee (Research platforms in the North Sea and Baltic Sea), https://www.fino-offshore.de/de/index.html, 2025.

Fontanella, A., Colpani, G., De Pascali, M., Muggiasca, S., and Belloli, M.: Assessing the impact of waves and platform dynamics on floating wind-turbine energy production, Wind Energy Science, 9, 1393–1417, https://doi.org/10.5194/wes-9-1393-2024, 2024.

Foussekis, D. and Mouzakis, F.: Wind resource assessment uncertainty for a TLP-based met mast, Journal of Physics: Conference Series, 2018, 012 018, https://doi.org/10.1088/1742-6596/2018/1/012018, 2021.

Fu, S., Jin, Y., Zheng, Y., and Chamorro, L. P.: Wake and power fluctuations of a model wind turbine subjected to pitch and roll oscillations, Applied Energy, 253, 113 605, https://doi.org/10.1016/j.apenergy.2019.113605, 2019.

Furevik, B. R. and Haakenstad, H.: Near-surface marine wind profiles from rawinsonde and NORA10 hindcast, Journal of Geophysical Research: Atmospheres, 117, https://doi.org/https://doi.org/10.1029/2012JD018523, 2012.

Gadde, S. N. and Stevens, R. J.: Effect of low-level jet height on wind farm performance, Journal of Renewable and Sustainable Energy, 13, https://doi.org/10.1063/5.0026232, 2021.

Gottschall, J., Gribben, B., Stein, D., and Würth, I.: Floating lidar as an advanced offshore wind speed measurement technique: current technology status and gap analysis in regard to full maturity, https://doi.org/10.1002/wene.250, 2017.

Gräfe, M., Pettas, V., Gottschall, J., and Cheng, P. W.: Quantification and correction of motion influence for nacelle-based lidar systems on floating wind turbines, Wind Energy Science, 8, 925–946, https://doi.org/10.5194/wes-8-925-2023, 2023.

Gutierrez, W., Ruiz-Columbie, A., Tutkun, M., and Castillo, L.: Impacts of the low-level jet's negative wind shear on the wind turbine, Wind Energy Science, 2, 533–545, https://doi.org/10.5194/wes-2-533-2017, 2017.

https://doi.org/10.5194/wes-2026-20
Preprint. Discussion started: 16 February 2026

Hahmann, A. N., Alonso De Linaje, N. G., and Mitsakou, A.: Assessing the wind energy technical potential of the North Sea - Final Project Report, Tech. rep., DTU Wind and Energy Systems, Roskilde, Denmark, ISBN 978-87-87335-65-2, 2023.

Hallgren, C., Aird, J. A., Ivanell, S., Körnich, H., Barthelmie, R. J., Pryor, S. C., and Sahlée, E.: Brief communication: On the definition of the low-level jet, Wind Energy Science, 8, 1651–1658, https://doi.org/10.5194/wes-8-1651-2023, 2023.

IEC 61400-12-1: International Standard IEC 61400: Wind turbines – Part 12-1: Power performance measurements of electricity producing wind turbines, 2022.

IEC 61400-50-3: IEC 61400 Wind energy generation systems - Part 50-3: Use of nacelle-mounted lidars for wind measurements, 2022.

Jacobsen, A. and Godvik, M.: Influence of wakes and atmospheric stability on the floater responses of the Hywind Scotland wind turbines, Wind Energy, 24, 149–161, https://doi.org/10.1002/we.2563, 2021.

Kalverla, P. C., Steeneveld, G. J., Ronda, R. J., and Holtslag, A. A.: An observational climatology of anomalous wind events at offshore meteomast IJmuiden (North Sea), Journal of Wind Engineering and Industrial Aerodynamics, 165, 86–99, https://doi.org/10.1016/j.jweia.2017.03.008, 2017.

Kim, J. Y., Oh, K. Y., Kim, M. S., and Kim, K. Y.: Evaluation and characterization of offshore wind resources with long-term met mast data corrected by wind lidar, Renewable Energy, pp. 41–55, https://doi.org/10.1016/j.renene.2018.06.097, 2019.

Larsen, G. C. and Hansen, K. S.: Full-scale measurements of aerodynamic induction in a rotor plane, Journal of Physics: Conference Series, 555, 12 063, https://doi.org/10.1088/1742-6596/555/1/012063, 2014.

Li, L., Liu, Y., Yuan, Z., and Gao, Y.: Wind field effect on the power generation and aerodynamic performance of offshore floating wind turbines, Energy, 157, 379–390, https://doi.org/10.1016/j.energy.2018.05.183, 2018.

Medici, D., Ivanell, S., Dahlberg, J. , and Alfredsson, P. H.: The upstream flow of a wind turbine: Blockage effect, Wind Energy, 14, 691–697, https://doi.org/10.1002/we.451, 2011.

Mikkelsen, T., Sjöholm, M., Astrup, P., Peña, A., Larsen, G., van Dooren, M. F., and Kidambi Sekar, A. P.: Lidar Scanning of Induction Zone Wind Fields over Sloping Terrain, Journal of Physics: Conference Series, 1452, 012 081, https://doi.org/10.1088/1742-6596/1452/1/012081, 2020.

Nunalee, C. G. and Basu, S.: Mesoscale modeling of coastal low-level jets: Implications for offshore wind resource estimation, Wind Energy, 17, 1199–1216, https://doi.org/10.1002/we.1628, 2014.

Olsen, B. T. E., Hahmann, A. N., Alonso-de Linaje, N. G., Žagar, M., and Dörenkämper, M.: Low-level jets in the North and Baltic Seas: Mesoscale Model Sensitivity and Climatology, https://doi.org/10.5194/egusphere-2024-3123, 2024.

Özinan, U., Liu, D., Adam, R., Choisnet, T., and Cheng, P. W.: Power curve measurement of a floating offshore wind turbine with a nacelle-based lidar, Journal of Physics: Conference Series, 2265, 042 016, https://doi.org/10.1088/1742-6596/2265/4/042016, 2022.

Peña, A., Gryning, S.-E., and Hasager, C. B.: Measurements and Modelling of the Wind Speed Profile in the Marine Atmospheric Boundary Layer, Boundary-Layer Meteorology, 129, 479–495, https://doi.org/10.1007/s10546-008-9323-9, 2008.

Peña, A., Mann, J., and Dimitrov, N.: Turbulence characterization from a forward-looking nacelle lidar, Wind Energy Science, 2, 133–152, https://doi.org/10.5194/wes-2-133-2017, 2017.

Peña, A., Mann, J., Angelou, N., and Jacobsen, A.: A Motion-Correction Method for Turbulence Estimates from Floating Lidars, Remote Sensing, 14, https://doi.org/10.3390/rs14236065, 2022.

Peña, A., Angelou, N., and Mann, J.: Impact of floating turbine motion on nacelle lidar turbulence measurements, Journal of Physics: Conference Series, 2767, 042 003, https://doi.org/10.1088/1742-6596/2767/4/042003, 2024.

https://doi.org/10.5194/wes-2026-20
Preprint. Discussion started: 16 February 2026

Robertson, A., Musial, W., Shields, M., Aubault, A., Ikari, M., and Kitzing, L.: Considerations for the global commercialization of floating offshore wind energy, Nature Reviews Clean Technology, 1, 734–749, https://doi.org/10.1038/s44359-025-00093-7, 2025.

Roots, M., Sullivan, J. T., and Demoz, B.: Mid-Atlantic nocturnal low-level jet characteristics: a machine learning analysis of radar wind profiles, Atmospheric Measurement Techniques, 18, 1269–1282, https://doi.org/10.5194/amt-18-1269-2025, 2025.

Sant, T., Bonnici, D., Farrugia, R., and Micallef, D.: Measurements and modelling of the power performance of a model floating wind turbine under controlled conditions, Wind Energy, 18, 811–834, https://doi.org/10.1002/we.1730, 2015.

Shaw, W. J., Berg, L. K., Debnath, M., Deskos, G., Draxl, C., Ghate, V. P., Hasager, C. B., Kotamarthi, R., Mirocha, J. D., Muradyan, P., Pringle, W. J., Turner, D. D., and Wilczak, J. M.: Scientific challenges to characterizing the wind resource in the marine atmospheric boundary layer, https://doi.org/10.5194/wes-7-2307-2022, 2022.

Simley, E., Angelou, N., Mikkelsen, T., Sjöholm, M., Mann, J., and Pao, L. Y.: Characterization of wind velocities in the upstream induction zone of a wind turbine using scanning continuous-wave lidars, Journal of Renewable and Sustainable Energy, 8, https://doi.org/10.1063/1.4940025, 2016.

Troldborg, N. and Meyer Forsting, A. R.: A simple model of the wind turbine induction zone derived from numerical simulations, Wind Energy, 20, 2011–2020, https://doi.org/10.1002/we.2137, 2017.

Tuononen, M., Sinclair, V. A., and Vihma, T.: A climatology of low-level jets in the mid-latitudes and polar regions of the Northern Hemisphere, Atmospheric Science Letters, 16, 492–499, https://doi.org/https://doi.org/10.1002/asl.587, 2015.

Van Sark, W. G., Van der Velde, H. C., Coelingh, J. P., and Bierbooms, W. A.: Do we really need rotor equivalent wind speed?, Wind Energy, 22, 745–763, https://doi.org/10.1002/we.2319, 2019.

Vratsinis, K., Marini, R., Daems, P.-J., Pauscher, L., van Beeck, J., and Helsen, J.: Impact of inflow conditions and turbine placement on the performance of offshore wind turbines exceeding 7 MW, https://doi.org/10.5194/wes-2025-32, 2025.

Wagner, R., Antoniou, I., Pedersen, S. M., Courtney, M. S., and Jørgensen, H. E.: The influence of the wind speed profile on wind turbine performance measurements, Wind Energy, 12, 348–362, https://doi.org/10.1002/we.297, 2009.

Wagner, R., Courtney, M., Gottschall, J., and Lindelöw-Marsden, P.: Accounting for the speed shear in wind turbine power performance measurement, Wind Energy, 14, 993–1004, https://doi.org/10.1002/we.509, 2011.

Wagner, R., Cañadillas, B., Clifton, A., Feeney, S., Nygaard, N., Poodt, M., Martin, C. S., Tüxen, E., and Wagenaar, J. W.: Rotor equivalent wind speed for power curve measurement – comparative exercise for IEA Wind Annex 32, Journal of Physics: Conference Series, 524, 012 108, https://doi.org/10.1088/1742-6596/524/1/012108, 2014a.

Wagner, R., Pedersen, T. F., Courtney, M., Antoniou, I., Davoust, S., and Rivera, R. L.: Power curve measurement with a nacelle mounted lidar, Wind Energy, 17, 1441–1453, https://doi.org/10.1002/we.1643, 2014b.

Wen, B., Tian, X., Dong, X., Peng, Z., and Zhang, W.: Influences of surge motion on the power and thrust characteristics of an offshore floating wind turbine, Energy, 141, 2054–2068, https://doi.org/10.1016/j.energy.2017.11.090, 2017.

Wen, B., Dong, X., Tian, X., Peng, Z., Zhang, W., and Wei, K.: The power performance of an offshore floating wind turbine in platform pitching motion, Energy, 154, 508–521, https://doi.org/10.1016/j.energy.2018.04.140, 2018a.

Wen, B., Tian, X., Dong, X., Peng, Z., and Zhang, W.: On the power coefficient overshoot of an offshore floating wind turbine in surge oscillations, Wind Energy, 21, 1076–1091, https://doi.org/10.1002/we.2215, 2018b.